Acta Materialia 200 (2020) 91–100

Contents lists available at ScienceDirect

Acta Materialia

journal homepage: www.elsevier.com/locate/actamat

Heterogeneous solute segregation suppresses strain localization in nanocrystalline Ag-Ni alloys

Zhiliang Pan [a], Frederic Sansoz [b,c,*]

[a] School of Mechanical and Electrical Engineering, Guilin University of Electronic Technology, Guilin, Guangxi Province 541004, China
[b] Department of Mechanical Engineering, The University of Vermont, Burlington, Vermont, United States
[c] Materials Science Program, The University of Vermont, Burlington, Vermont, United States

ARTICLE INFO

Article history:
Received 4 March 2020
Revised 26 August 2020
Accepted 27 August 2020
Available online 2 September 2020

Keywords:
Nanostructured materials
Heterogeneous segregation
Homogeneous segregation
Strain localization
Atomistic simulations

ABSTRACT

Solute segregation to individual grain boundaries is used by design to produce strong and stable nanocrystalline metallic alloys. Grain-boundary segregation, however, is known to cause adverse embrittlement effects from a strain-localization failure mechanism that imposes significant material limitations for structural applications. Here, using atomistic simulations, it is discovered that heterogeneous Ni segregation in nanocrystalline Ni-mixed Ag alloys dramatically shuts down localized shear bands during plastic deformation, while simultaneously increasing the tensile strength. Nanocrystalline Cu-mixed Ag metals are predicted to exhibit standard homogeneous Cu segregation and a tensile strength that saturates above a solute concentration of 8 at.% due to glass-like shear localization induced by grain boundaries. By contrast, it is found that heterogeneous Ni segregation in nanocrystalline Ag-Ni alloys forms solute-rich clusters along interfaces leading to strain delocalization at high strain and continuous strengthening at high solute concentrations up to 15 at.%. This study reveals the importance of heterogeneous versus homogeneous segregation behaviors on strain localization and points to a fundamentally new strategy to design failure-resistant nanostructured materials through grain boundary segregation engineering.

© 2020 Acta Materialia Inc. Published by Elsevier Ltd. All rights reserved.

1. Introduction

A reduction of grain size into the nanometer range is known to dramatically increase the yield strength of materials [1–3], called the Hall-Petch strengthening effect. However, grain-boundary (GB) strengthening ceases at extremely fine grain sizes as the underlying deformation mechanism transitions from dislocation-based to GB-dominated plasticity [4–8] and glass-like deformation [9]. GB solute segregation has proven to be an efficient strategy to reduce GB-mediated plastic deformation [10–13] and therefore holds promise to achieve continuous metal hardening up to the smallest grain size. Recently, Hu et al. [14] have demonstrated that Mo segregation stabilized GBs in nanocrystalline Ni-Mo alloys at high Mo concentration, associated with a resurgence of Hall-Petch strengthening at grain sizes below 10 nm. Transmission electron microscopy of the smallest grains provided direct experimental evidence for a pronounced shift from GB plasticity to intragranular planar slip bands with increased Mo segregation.

Current literature suggests two categories of solute segregation behavior at GBs. The first is *homogeneous* segregation, where solute atoms are distributed uniformly along the interfaces at all concentrations, with GB segregation of Zr in Cu [15], W in Ni [16,17] and Cu in Ag [13,18] as representative examples. The second is *heterogeneous* segregation, a unique behavior where solute atoms cluster along some GB regions, whereas other regions are left solute-free. This phenomenon was recently found in GB segregation of Ta in Cu [19], Au in Pt [20,21] and Ni in Ag [22]. Yet most investigations of mechanical properties have been focused on nanocrystalline alloys governed exclusively by homogeneous segregation.

Furthermore, theory and simulations speculate that the potential of segregating elements to either weaken or strengthen individual GBs governs the type of embrittlement mechanism in nanocrystalline alloys [23]. In the case of a GB embrittling element, a study in nanocrystalline Pt metals has found that GB segregation of 10 at.% Au alloying element promoted brittle-like behavior and fast cracking [24]. Surprisingly, however, the study revealed that a smaller concentration of 5 at.% Au made it possible for the alloy to recover some ductility at the same grain size from crack arrest at triple junctions, due to heterogeneous GB segregation. In contrast, the deterioration of toughness and ductility in pure metals

* Corresponding author.
E-mail address: frederic.sansoz@uvm.edu (F. Sansoz).

https://doi.org/10.1016/j.actamat.2020.08.074
1359-6454/© 2020 Acta Materialia Inc. Published by Elsevier Ltd. All rights reserved.

with uniform nanosized grains is more generally associated with strain localization leading to catastrophic failure from shear banding [25–34]. In nanocrystalline alloys containing GB strengthening elements, such as Ag-Cu alloys [35] and $Al_{85}Ni_{10}Ce_5$ alloy [36], strong shear localization was found after the onset of plasticity induced by indentation. Remarkably, Balbus et al. [36] have observed a reduction of shear localization and increase in strength that resulted from GB segregation of Ni and Ce solutes after low-temperature annealing, which led to the formation of an amorphous phase along the interfaces. So far, however, the incidence of heterogeneous solute segregation on shear localization and shear-band formation remained unknown.

The present study reveals several fundamental differences in GB segregation strengthening between nanocrystalline Ag-Cu and Ag-Ni alloys, studied by hybrid Monte Carlo (MC) and molecular dynamics (MD) simulations. Nanocrystalline Ag-Ni alloys are of special interest because recent theoretical models [22] predicted that GB segregation in Ag containing small Ni concentrations ($\leq$ 2 at%) is intrinsically heterogeneous. Our atomistic simulations show that both Cu and Ni segregations significantly improve strength in nanocrystalline Ag, but the dependence on solute concentration is markedly different. The strengthening effect of homogeneous Cu segregation saturates as Cu concentration increases due to nucleation and propagation of strain-localized shear bands. On the contrary, heterogeneous Ni segregation suppresses the strain localization at high strain, which helps in maintaining continuous strengthening with increasing solute concentration. Atomistic simulations and a new mechanistic theory are used to show how Ni-rich clusters along interfaces can suppress GB-localized shear bands. The present study demonstrates the striking merit of heterogeneous GB segregation as a fundamentally new mechanism for concomitantly strengthening and toughening nanocrystalline alloys.

2. Simulation methods

Hybrid MC/MD simulations were performed with the software LAMMPS [37] using an embedded-atom method potential for Ag-Cu alloys [38] and a newly developed Finnis-Sinclair interatomic potential for Ag-Ni alloys developed in our previous work [22]. Both potentials were fitted on extensive ab-initio databases; however, values for Ni segregation energy and Ni-Ni dipole formation at GBs were only included in the later. A nanocrystalline atomistic model was constructed by the Voronoi tessellation method in a 30 $\times$ 30 $\times$ 30 nm^3 cubic box with periodic boundary conditions applied in all three spatial directions. Because nanocrystalline Ag easily forms a high density of twin boundaries due to its low stacking-fault energy [18], we added parallel twin boundaries with a constant spacing of 2.8 nm in each grain. The experimental study of Ke et al. [18] has found that a transition from classical dislocation-based Hall-Petch strengthening to GB-stress controlled plasticity occurred at twin spacings below 8 nm in Ag polycrystals of 45 nm in average grain diameter, or a ratio of twin size over grain diameter of ~0.15. By extrapolating this result to the simulated 6-nm grain size, the TB spacing threshold becomes 1.4 nm in Ag. Therefore, we chose a TB spacing of 2.8 nm to be close to this transition without annihilating the dislocation-based plasticity mechanisms.

The potential energy of the as-constructed model was minimized to its local minimum value by conjugate-gradient algorithm. Then the model was well equilibrated by being relaxed at 450 K for 100 ps, cooled to 300 K in 50 ps, and held at 300 K for another 50 ps, with a Nose-Hoover thermostat and a Parrinello-Rahman barostat kept under zero pressure. Finally, the model was equilibrated further at 500 K (which is close to the annealing temperature of Cu-segregated nanocrystalline-nanotwinned Ag in a previous study [18]) under zero pressure for 50 ps to prepare for the subsequent MC doping process. The timestep was 2 fs. Fig. 1a shows the equilibrated structure containing 46 grains (average grain size of ~6 nm) and ~1,600,000 atoms, as colored by adaptive common neighbor analysis (CNA) [39] in the visualization software OVITO [40]. Furthermore, the model was doped every 100 MD steps with either Cu or Ni atoms by MC method in a variance-constrained semigrand canonical ensemble [41]. The global composition of solute atoms was fixed to different concentrations up to 15 at.% in small increments by adjusting the initial chemical potential difference [42]. The simulations were found to converge to equilibrium after 1 million steps, since additional simulation steps led to negligible structural and chemical changes. Before tensile deformation, the doped models were quenched from 500 K to 300 K for 100 ps and then kept at 300 K for another 100 ps at zero pressure with a Nose-Hoover thermostat and a Parrinello-Rahman barostat. The uniaxial tensile deformation was simulated by stretching the domain in the X direction at a strain rate of 10^8 s^{-1} and a constant temperature of 300 K while maintaining zero pressure in Y and Z directions.

3. Results

3.1. Homogeneous versus heterogeneous solute segregations

It is found from Fig. 1b that, at a concentration of 8 at.% Cu, the majority of Cu atoms are distributed uniformly along GBs with some solute remaining inside the grains. This result points to homogeneous segregation at equilibrium. By contrast, at the same concentration of Ni solute, Fig. 1c reveals that all Ni atoms are segregated into GBs, but some GBs are more slightly segregated than others and most Ni atoms have formed Ni-rich clusters in the GB network. Fig. 1d and Supplementary Material Movie S1 present the three-dimensional distribution of Ni-rich clusters in the simulation box, in which each cluster is defined as a group of atoms containing more than one hundred continuously bonded Ni atoms (within a cutoff distance of 3 Å) and their closest atom neighbors. They confirm that the segregation of Ni solute into Ag GBs is strongly heterogeneous. For homogeneous Cu segregation, this method finds no apparent cluster because Cu atoms are either bonded in small groups of 2–3 atoms or isolated.

Furthermore, in Fig. 2, we quantitatively analyzed the fraction and chemistry of the GB network, as a function of global solute concentration, for the two nanocrystalline alloys. First, Fig. 2a shows that the GB atom fraction increases identically with both Cu and Ni additions. Second, Fig. 2b indicates that in nanocrystalline Ag-Ni alloys, the GBs attain a high fraction of Ni-rich clusters that also increases with increasing Ni composition, whereas no Cu cluster exists in Ag-Cu alloys at all concentrations. Here, the fraction of solute-rich clusters was determined as the total number of cluster atoms divided by the total number of atoms in the sample. Third, we computed the GB solute concentration from the ratio of solute atoms globally segregated to the GB network over the total number of GB atoms. A caveat in this analysis is that GB solute concentrations in nanocrystalline Ag-Ni alloys excluded the atoms present in Ni-rich clusters, to accurately compare the local chemistries inside individual GBs after Cu and Ni segregations. Interestingly, due to the formation of Ni clusters, Fig. 2c shows that the Ni solute concentration at GBs forms a plateau at 5 at.% composition and becomes significantly smaller than the GB solute concentration in nanocrystalline Ag-Cu alloys. These results suggest that the difference in plasticity mechanisms resulting from homogeneous versus heterogeneous solute segregations could be strongly dependent on the fraction and solute concentration of GBs, as well as the fraction of solute-rich clusters.

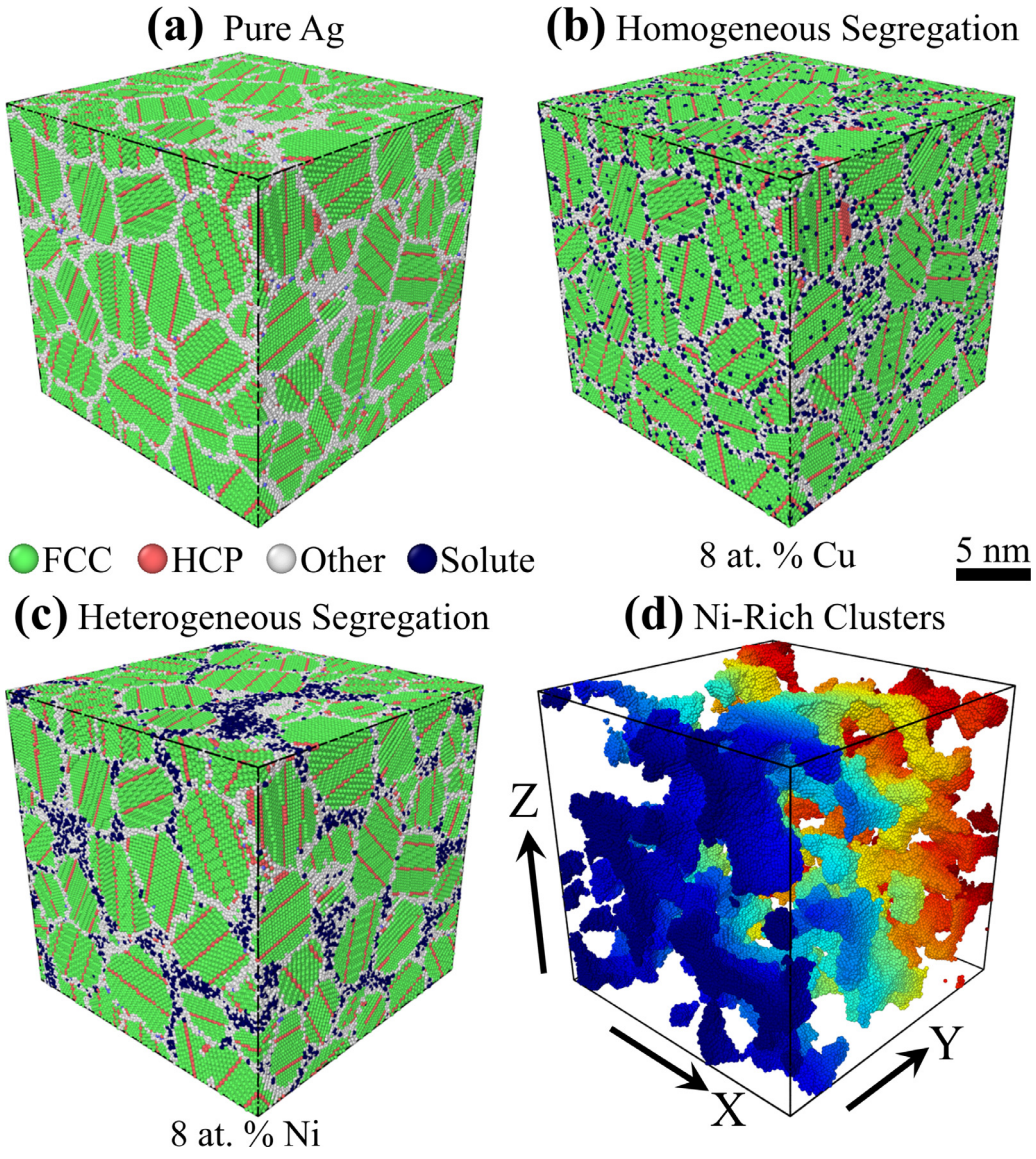

Fig. 1. Equilibrium configurations of nanostructured metals in **(a)** pure Ag, **(b)** Ag alloy with homogeneous Cu segregation, and **(c)** Ag alloy with heterogeneous Ni segregation. Atoms with face-centered cubic (FCC), hexagonal close-packed (HCP), and other crystal arrangements are colored in green, red and white colors, respectively. Solute atoms (Cu or Ni) are highlighted in dark blue. **(d)** Three-dimensional rendering of the distribution of Ni-rich clusters formed at a content of 8 at.% Ni, with atoms colored according to the Y coordinates. (For interpretation of the references to colour in this figure legend, the reader is referred to the web version of this article.)

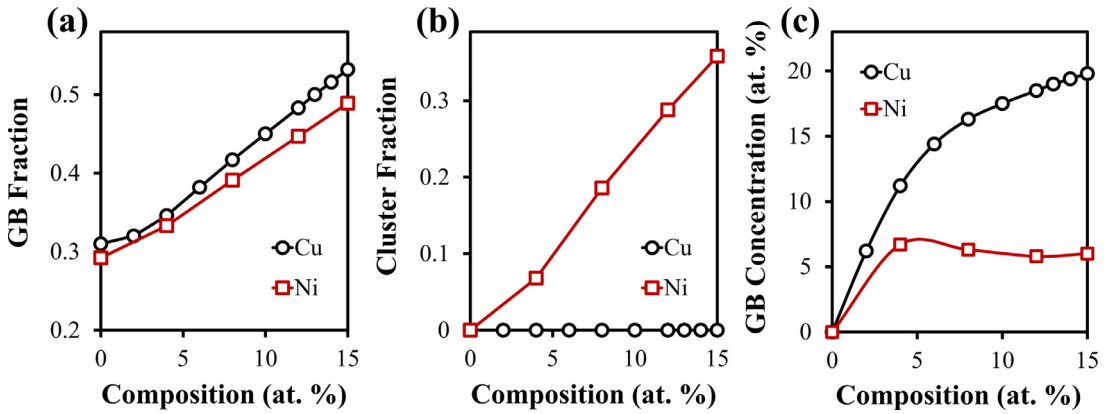

Fig. 2. Grain-boundary (GB) analysis of the polycrystal model in Fig. 1 as a function of total solute concentration (Cu vs. Ni segregations). (a) Total fraction of GB atoms. (b) Fraction of solute-rich cluster atoms. (c) GB solute concentration.

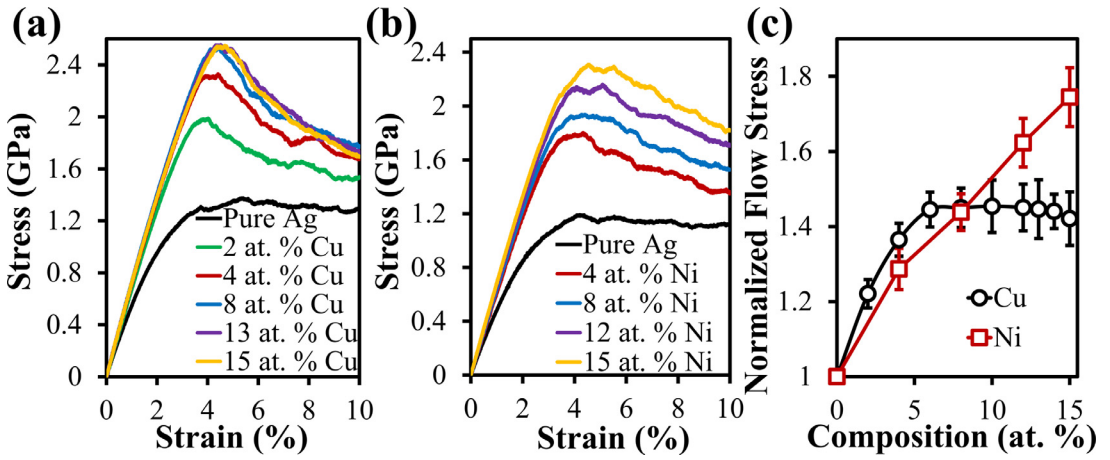

Fig. 3. Simulated tensile stress-strain curves of **(a)** Cu-segregated nanocrystalline Ag and **(b)** Ni-segregated nanocrystalline Ag. **(c)** Normalized flow stress as a function of solute composition, showing that Cu-segregation strengthening reaches a stress maximum while Ni strengthening shows no saturation with composition up to 15 at.%.

3.2. Solute-segregation dependence on tensile strength

The simulated stress-strain curves represented in Figs. 3a and 3b show more than 180% increase in tensile strength by adding 15 at.% concentrations of Cu and Ni solutes, respectively, compared to that of pure nanocrystalline Ag. GB plasticity rapidly dominates the deformation in pure Ag (Supplementary Materials Fig. S1). The apparent solute strengthening up to 15 at.% is associated with a pronounced elimination of GB plasticity from the segregation of Cu (Supplementary Materials Fig. S2) and Ni (Supplementary Materials Fig. S3) along interfaces. This result agrees with past atomistic simulation studies on the effects of solute segregation on plastic yielding with GB strengthening elements [13,18,43].

It is worth noting that Figs. 3a and 3b show stress-strain curves predicted from two different interatomic potentials. Although the two curves obtained for pure Ag resemble each other, the associated plastic flow stresses predicted are noticeably higher from the Ag-Cu potential than the Ag-Ni potential. Therefore, to maintain consistency, we studied the normalized flow stress as a function of solute composition in Fig. 3c where normalized flow stress is defined as the stress average between 7% and 10% tensile strain divided by the average flow stress of pure Ag in this range. Quantitative analysis of normalized flow stresses, as a function of solute concentration, suggests a fundamental difference in strengthening behavior between Cu and Ni solutes. Results in Fig. 3c show a rapid increase in plastic flow stresses reaching a maximum at a global concentration of 8 at.% in Cu. In marked contrast, the plastic flow stress increases continuously with Ni solute concentration, without saturation for the studied range of Ni compositions up to 15 at.%. In other words, our atomistic simulations provide direct numerical evidence that homogeneous segregation and heterogeneous segregation give rise to fundamentally different mechanical behaviors in nanocrystalline Ag containing GB-segregated strengthening elements.

3.3. Shear-localization and delocalization mechanisms

To further demonstrate that Cu segregation and Ni segregation impact the mechanical behavior differently, the local atomic shear strains in pure Ag, Cu-segregated Ag, and Ni-segregated Ag, after a total of 10% applied deformation are computed in Fig. 4. Here, the atomic shear strain is in fact the von Mises shear strain defined based on the six strain components of each atom. The strain components of an atom were calculated from the relative motion of its neighbors between the current configuration and the configuration right before deformation. Therefore, the calculated atomic shear strain measures the local deformation around each atom resulted from the global tensile deformation, regardless of the atom position (in GBs or crystalline lattices). Fig. 4a shows that a localized shear band running through the sample is formed in Cu-segregated nanocrystalline Ag by a combination of GB sliding and intragranular crystal slip. On the contrary, no shear band appears to run through the Ni-segregated model after 10% deformation in Fig. 4b.

Furthermore, Fig. 5 and Movie S2 represent the reduced shear strain in the XZ plane with strain in each bin averaged throughout the Y direction. A diffused shear band is predicted for the two models in pure Ag indicating that, despite small differences in flow stress, the potentials used predict identical plastic deformation mechanisms after plastic yielding. Fig. 5a shows that the local shear strain distribution changes gradually to strain-localization when increasing the Cu solute concentration up to 15 at.%, which suggests strong segregation-induced shear banding through the Y direction. Surprisingly, however, an opposite trend is found for the segregation of Ni solute in nanocrystalline Ag. At a global composition of 4 at.% Ni, Fig. 5b shows that the initial shear band is still visible like that observed with 4 at.% Cu. However, it is evidenced in the same figure that the shear band disappears completely at global Ni compositions of 8 at.% or higher. Also, Fig. 5b shows the reduced shear strain map in the XY plane with strain in each bin averaged throughout the Z direction, clearly demonstrating that no localized shear band has formed in the other direction either. The strongest evidence of strain delocalization in nanocrystalline Ag with 15 at.% Ni, which is totally absent in the Cu-segregated counterpart, is dynamically displayed in Supplementary Materials Movie S2.

The atomic-scale mechanism responsible for strain delocalization in materials with heterogeneous solute segregation is addressed in Fig. 6. In Fig. 6a, GB plasticity in Cu-segregated nanocrystalline Ag is shown to initiate shear banding where maximum shear deformation occurs along GBs making a ~45° angle with the tensile loading direction, as indicated by arrows 1–3. In Ni-segregated nanocrystalline Ag, however, the interface strengthening induced by Ni clustering plays an increasingly important role as Ni concentration increases, because Ni clusters have extremely low shear strain compared to other regions, as highlighted by arrows 4–5 in Fig. 6b. In addition, the local shear deformation formed along GBs stops on these clusters, as shown by arrows 6–7, thereby limiting the formation of an extended shear band like that in Cu-segregated nanocrystalline Ag. Furthermore, despite a small

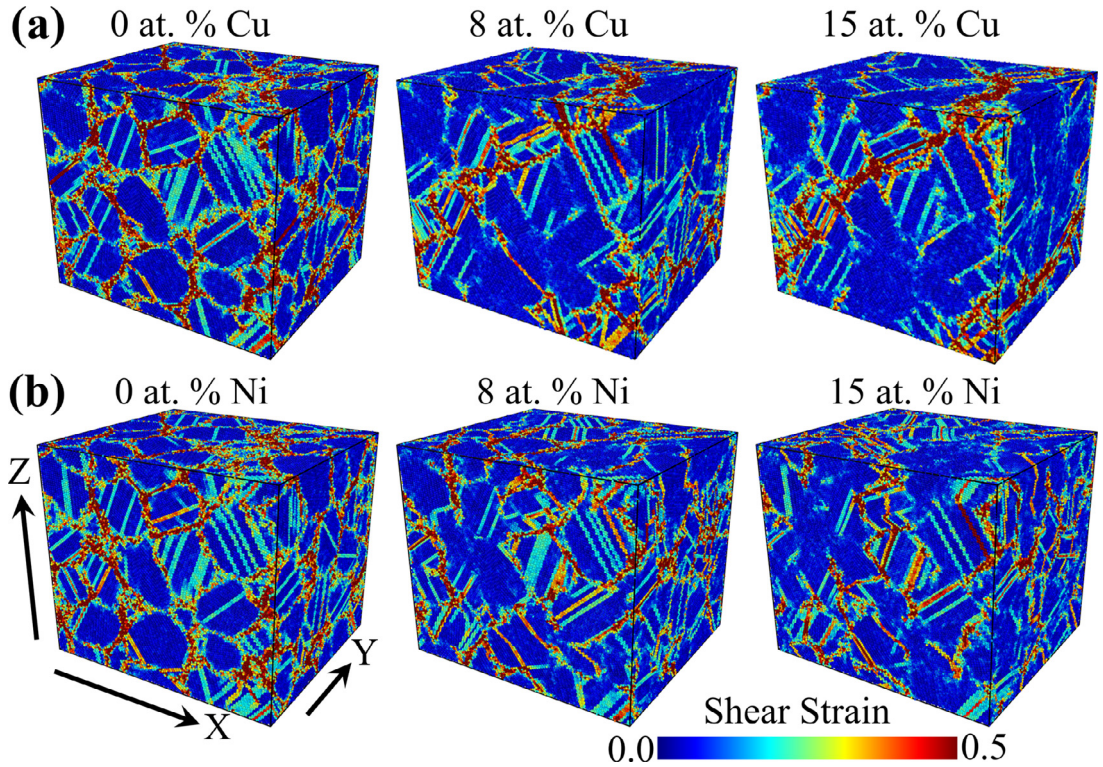

Fig. 4. Atomic von-Mises shear strain calculations at a tensile strain of 10% inside (a) Cu-segregated nanocrystalline Ag and (b) Ni-segregated nanocrystalline Ag, demonstrating that a shear band tends to form preferentially in Cu-segregated materials, which is absent in Ni-segregated ones at large applied strains.

grain size of 6 nm and a volume fraction of GB atoms estimated to be ~30%, we find that TBs and dislocations contribute to plasticity in our models. Based on Figs. 4 and 6, however, dislocation-based plasticity did not seem to be influenced by the type of solute, because most solutes are segregated to GBs. Therefore, our atomistic simulations strongly suggest that Ni clustering at triple junctions and interfaces leads to strain delocalization and sustained strengthening with increasing Ni concentration.

Geometric effects play a key role in the suppression of strain localization with Ni segregation, whereas GB chemistry effects on strength are more predominant in homogeneous segregation (Cu) than in heterogeneous segregation (Ni). For example, as shown in Fig. 5b, at Ni concentration of 4 at.%, a global shear band is still observed. It is only when the size of Ni-rich clusters is large enough that the shear localization is suppressed and strength increases. On the contrary, strength level saturates, and shear localization increases in the case of Ag-Cu alloys, because the GB solute concentration increases much faster than in Ag-Ni alloys (Fig. 2c). Therefore, this analysis requires us to quantify how the GB shear strength evolves with GB or shear-band length (geometric effect) and GB solute concentration (chemistry effect), as addressed independently in Sections 3.4 and 3.5, respectively.

3.4. Relationship between maximum GB shear strength and shear-band length

We have numerically studied how the maximum GB shear strength varies with the GB length, or the longest possible shear band length along GBs, denoted as L in the following, by performing a series of atomistic simulations of shearing of a bicrystal as shown in Fig. 7a. In this model, we consider a GB interface of finite length L intersected by a crystalline phase at both ends, in order to confine the shear localization induced by GB sliding within the GB length. Ten models were created with different lengths L. Shear deformation was applied to this configuration with the bottom region fixed, while the upper region was displaced at a constant velocity until a total shear strain of 10% was reached. The velocity was chosen such that the shear strain rate of the deformed region was 10^8 s^{-1}. Free surface boundary conditions were applied in the vertical direction and periodic boundary conditions in other directions. Before deformation, the model was equilibrated for 100 ps by MD with an NPT integration at a temperature of 300 K with zero pressure in all directions with periodic boundary conditions. During deformation, MD with an NVT integration at 300 K was performed to equilibrate the atoms in the deformed region in response to the applied shear stress. Fig. 7b shows that the maximum GB shear strength obtained by pure shear deformation, denoted τ_{GB}, follows a Hall-Petch-like relationship such as

$$\tau_{GB} = \tau_{GB}^{c} + \frac{k}{\sqrt{L}} \tag{1}$$

where τ_{GB}^{c} is a critical friction stress for sliding an infinitely long GB and k is a constant, both of which are dependent upon the GB chemistry.

3.5. Relationship between maximum GB shear stress and GB solute concentration

From the solute-concentration dependence of flow stress simulated in Fig. 3c, it can be hypothesized that the maximum GB shear strength is strongly dependent on local solute concentration. To quantify this relationship, we carried out a series of atomistic simulations to compute the maximum GB shear strength and GB solute concentration, from another type of bicrystal as shown in Fig. 8a. Free surface boundary conditions were applied in the vertical direction and periodic boundary conditions in other directions, such that the GB length simulated in the bicrystal was infinite and unconstrained by crystal phases. Therefore, the shear band length was kept constant, while the solute composition was varied, which

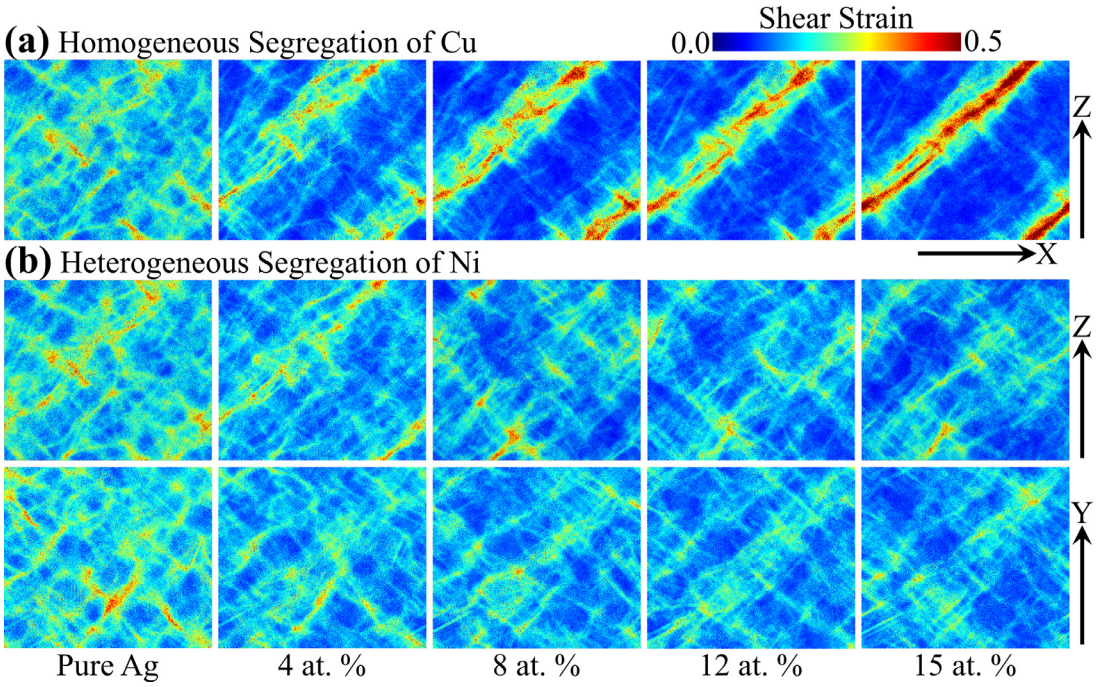

Fig. 5. Reduced shear strain on the X-Z plane under tensile strain of 10% in (a) Cu-segregated nanocrystalline Ag and (b) Ni-segregated nanocrystalline Ag simulated by MD. The reduced strain map on the X-Y plane is also shown for Ni-segregated Ag. An increase in homogeneous Cu concentration promotes strain localization whereas increasing heterogeneous Ni segregation tends to suppress it. (For interpretation of the references to colour in this figure legend, the reader is referred to the web version of this article.)

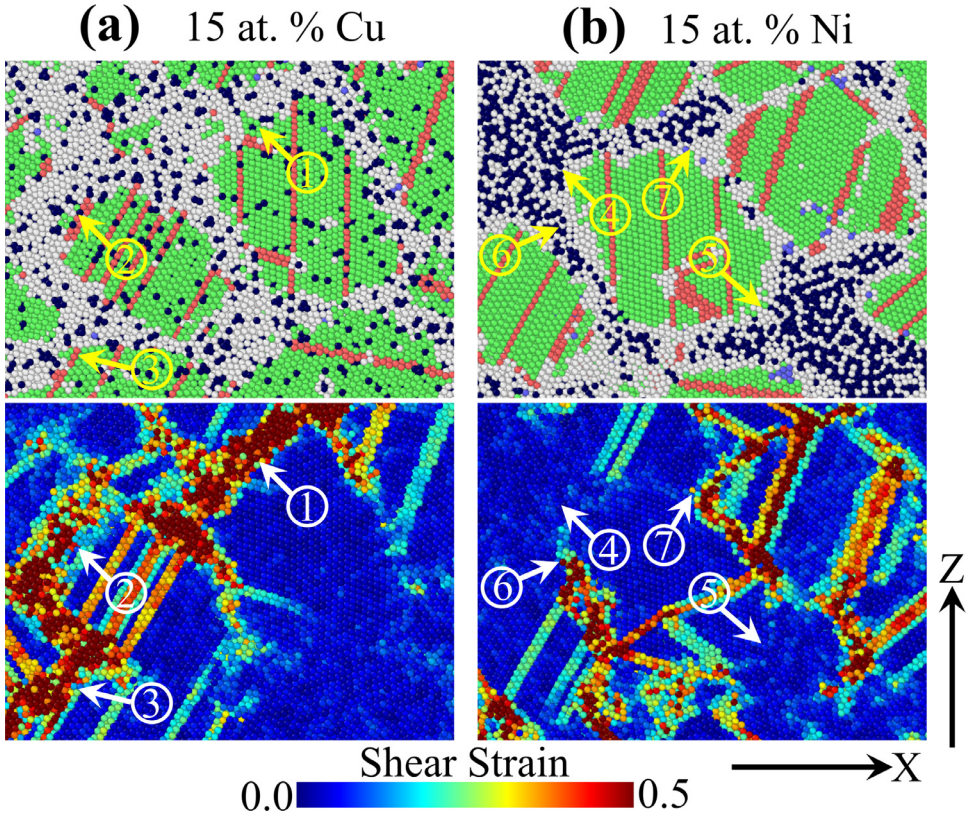

Fig. 6. Close-up atomistic snapshots of plastic deformation mechanisms under tensile strain of 10% and solute concentration of 15 at.% in (a) Cu-segregated nanocrystalline Ag and (b) Ni-segregated nanocrystalline Ag colored according to the common-neighbor analysis with solute atoms highlighted as dark blue (top) and local atomic shear strain (bottom). The strain is localized mostly inside Cu-segregated GBs marked as 1, 2 and 3 in (a), but is stopped by Ni-rich clusters marked as 4, 5, 6 and 7 in (b). (For interpretation of the references to colour in this figure legend, the reader is referred to the web version of this article.)

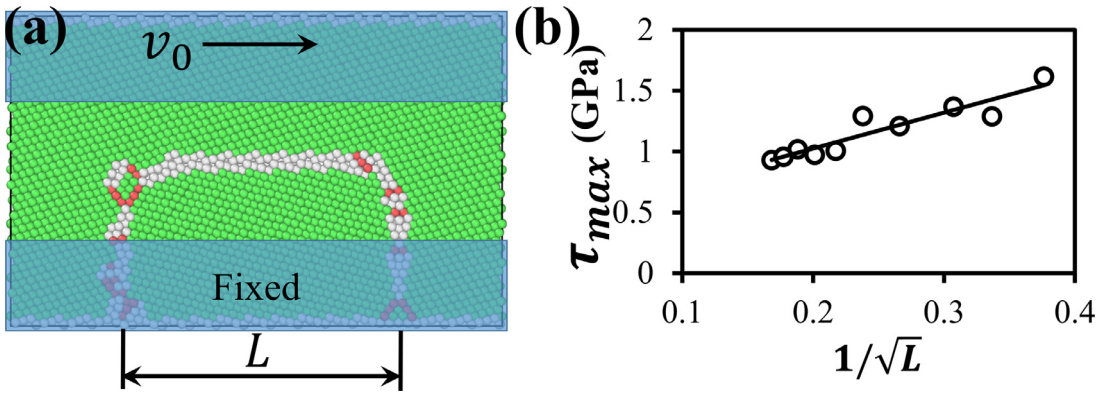

Fig. 7. Relationship between maximum GB shear strength and GB length from MD simulation on bicrystal. (a) Atomistic model used. During the deformation, the bottom shaded part is fixed while the upper shaded part is displaced at a constant speed. (b) The maximum GB shear stress (τ_{max}) as a function of length L.

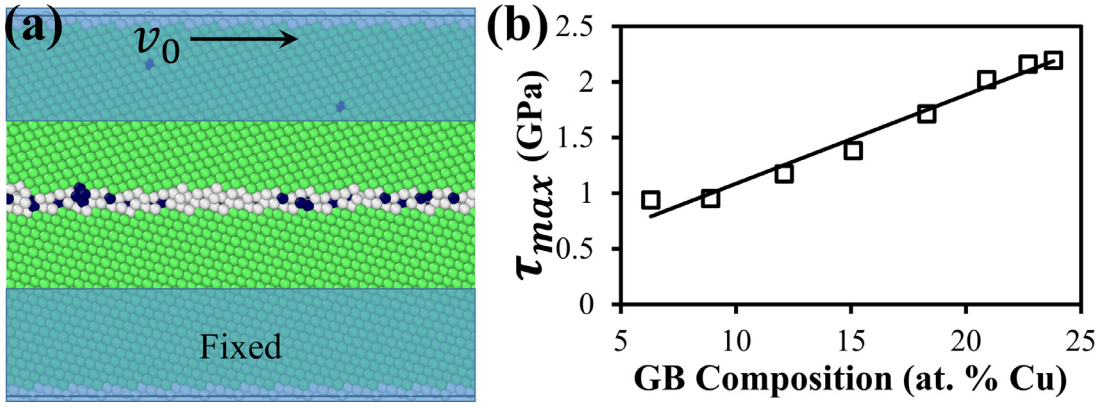

Fig. 8. Relationship between maximum GB shear strength and GB solute concentration in a bicrystal from MD simulation. (a) Atomistic model used. During the deformation, the bottom shaded part is fixed while the upper shaded part is displaced at a constant speed. The GB area is constant and periodic. (b) The maximum GB shear stress (τ_{max}) as a function of GB solute composition.

was not possible to control in the nanograined simulations presented above. After equilibration with NPT integration at 300 K under zero pressure for 100 ps, the temperature was gradually increased to 500 K in 50 ps and held at this temperature for 100 ps. Then the sample was doped with the same MC technique used to produce the nanocrystalline alloy models, with the global composition increased up to 15 at.% Cu in small increments. This method resulted in a GB solute concentration of Cu ranging from 5 at.% to 20 at.%, which was adequate in comparison to the GB solute concentrations predicted in the polycrystal model (> 6 at.% Cu). The doped bicrystal was quenched to 300 K and then deformed under pure shear as described above. The maximum shear stress is plotted against GB solute composition in Fig. 8b. It is shown in this figure that the change in GB shear strength relates linearly to the GB solute concentration, C_{GB}, within the range of compositions studied:

$$\Delta\tau_{GB} = \beta C_{GB} \tag{2}$$

where β is a measure of the GB strength sensitivity to the GB solute concentration, independent of the GB length.

4. Discussion

4.1. Shear-band strengthening theory for nanocrystalline metals

The present study reveals that, when the solute concentration is increased, the onset of shear localization from homogeneous GB segregation significantly impedes segregation-induced strengthening in nanocrystalline Ag-Cu alloys, whereas heterogeneous segregation in nanocrystalline Ag-Ni alloys gives rise to strain delocalization and continuous GB strengthening simultaneously. This competition between strain-localization softening and GB-segregation strengthening can be captured with a mechanistic model as follows. Our MD simulations suggest that the high fraction of GBs in nanocrystalline Ag with a 6-nm grain size promotes larger shear banding and localization than the plasticity mechanisms studied in nanocrystalline Ag with larger grain sizes and smaller GB fractions; see for example Ke et al. [18]. Furthermore, Fig. 2a indicated that the GB atom fraction increases monotonically with an increase in either Cu or Ni concentrations, which is expected to accelerate strain localization. In fact, an increase in GB fraction facilitates shear band propagation because the shear strain path becomes more continuous through GBs. Apparently, this result agrees with the literature on plastic deformation of metallic glass-crystal composites where it is found that deformation shear bands propagate easily through the glassy phase and are blocked by embedded crystals [44–46]. The glass-crystal composite model for shear banding shows that strength relates linearly to the crystalline phase volume fraction. In nanocrystalline Ag-Ni alloys, however, the GBs contain a high fraction of Ni-rich clusters that also increases with increasing Ni composition, as shown in Fig. 2b, whereas no cluster exists in Cu-segregated Ag alloys. The Ni clusters are found to play an important geometric role in reducing the length of the shear band passing through GBs. As a result, the impact of GB fraction on shear band formation breaks down with heterogeneous Ni segregation.

It should be noted that Voronoi tessellation does not always generate the most realistic grain structures, especially those resulting from grain growth. However, a study by Gruber et al. [47] has

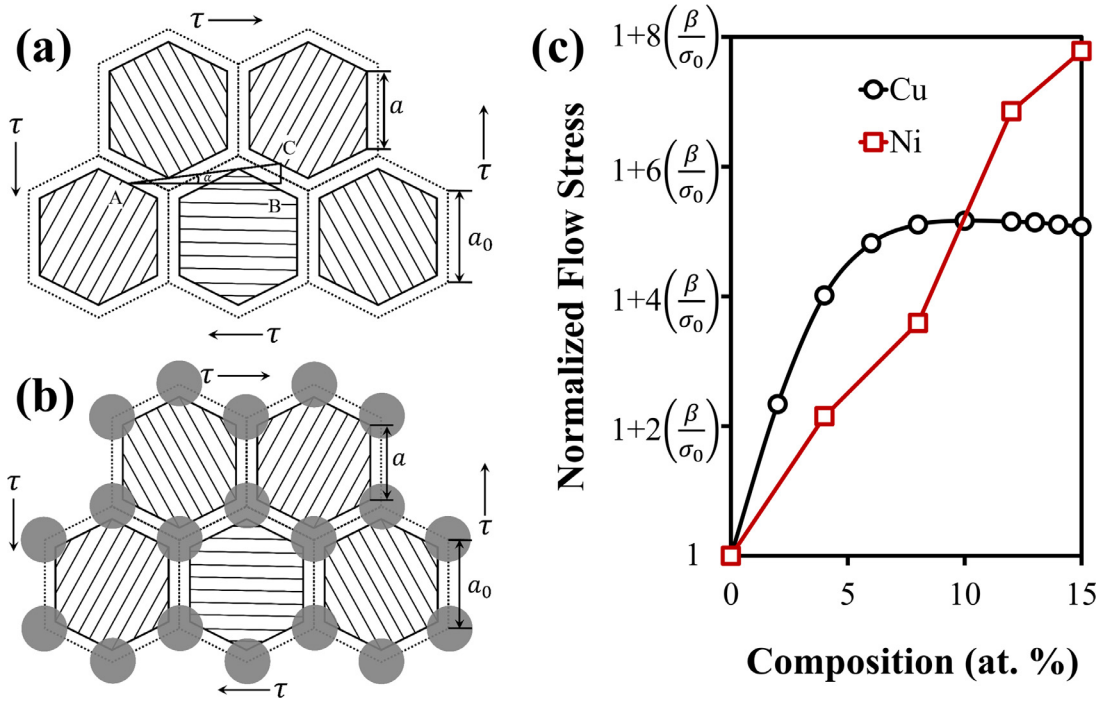

Fig. 9. Two-dimensional theoretical model of shear-band formation in nanocrystalline alloys with (a) homogeneous Cu segregation and (b) heterogeneous Ni segregation. Heterogeneous segregation is modeled by solute-rich clusters of equal size at each GB triple junction, showing how the shear-band length and shear strain path are shortened by these clusters. (c) Theoretical estimates based on the proposed model (Eq. (8)) for the normalized flow stress as a function of solute composition with Cu and Ni segregation behaviors. The two theoretical trends for Cu-segregated and Ni-segregated nanocrystalline Ag metals agree well with direct MD simulation results presented in Fig. 3c.

shown little difference in the macroscopic mechanical response between the NC structures generated with Voronoi tessellation method and that with grain growth method. Although differences exist in the resolved contribution to strain from different deformation mechanisms, this difference should not affect our conclusion since Ag-Cu and Ag-Ni alloys all started from the same configuration.

In the proposed model, we assume that the flow strength of nanocrystalline metals failing by localized shear bands is governed by the longest shear band, or possible shear strain path, through the glassy phase or GB region. For simplicity, we consider a two-dimensional nanocrystalline configuration with hexagonal grains of the same size, as schematically illustrated in Fig. 9a. A linear shear-band is assumed to develop inside the GB region between a group of 4 grains. The path is mostly linear because of the small grain size. Furthermore, as shown in Figs. 4(a) and 5(a), tiny linear shear bands that form at low Cu composition were found to gradually converge to a global thin shear band which is still linear at high Cu composition. For nanocrystalline metals studied in this work, the length of the longest shear band, L, depends on grain size and GB thickness. In our model, the shear-strain path inside the GB region extends between points A and C in Fig. 9a and is blocked by neighboring crystalline grains. The angle between the shear band and the applied shear stress τ ($\angle$CAB) is denoted as α, and the GB volume fraction as f_{GB}. Geometrically, we have

$$f_{GB} = 1 - (a/a_0)^2 \tag{3}$$

$$\alpha = \operatorname{atan}\left(\frac{4a - 3a_0}{\sqrt{3}a_0}\right) \tag{4}$$

$$L = \frac{\sqrt{3}a_0}{2\cos\alpha} + \frac{2\sqrt{3}(a_0 - a)}{\cos(60^\circ - \alpha)} \tag{5}$$

where a represents the actual crystal size and a_0 the standard grain size assuming no GB thickness, as shown in Fig. 9a. From Eqs. (3)-(5), the model predicts that increasing the GB fraction for a fixed grain size a_0 decreases the values of both a and α, but increases the shear-band length L, which is consistent with the experimental and computational results. Furthermore, the resolved shear stress acting on the shear band (line AC) is expressed as

$$\tau_{AC} = \frac{\tau \cdot AB \cdot \cos\alpha - \tau \cdot BC \cdot \sin\alpha}{AC} = \tau(\cos\alpha)^2 - \tau(\sin\alpha)^2 = \tau\cos 2\alpha \tag{6}$$

4.2. Application to homogeneous solute segregation

In the polycrystal model (Fig. 9), it should be emphasized that the geometric parameters α and L, material properties τ_{GB}^c and k in Eq. (1) and shear-band strength τ_{AC} in Eq. (6) should be altered by the GB solute concentration, C_{GB}. As a first-order approximation, however, we consider that the dependence of α and L on C_{GB} is negligible and that the primary effect of GB segregation is on k and τ_{AC}. This approximation satisfies the predictions from Eq. (2) where the shear band length in the bicrystal was also considered constant and independent of C_{GB}. For nanocrystalline alloys, we therefore propose to divide the flow stress into two terms, with one term related to the polycrystal strength in the pure metal and the other to combined GB chemistry and geometric (shear localization) effects, such as:

$$\sigma = \sigma_0 + \frac{\beta C_{GB}}{\cos 2\alpha\sqrt{L}} \tag{7}$$

Here σ_0 is the flow stress of pure nanocrystalline Ag, the change of flow stress due to GB segregation is described by the second term of the equation. C_{GB} remains the GB solute concentration in the entire GB region, and β is the coefficient describing

how fast the flow stress increases with GB concentration. The normalized flow stress is therefore

$$\frac{\sigma}{\sigma_0} = 1 + \frac{\beta}{\sigma_0}\left(\frac{C_{GB}}{\cos 2\alpha\sqrt{L}}\right) \quad (8)$$

Both parameters L and α are governed by the grain size a_0 and the GB volume fraction f_{GB}. For homogeneous Cu segregation in nanocrystalline Ag, both C_{GB} and f_{GB} were retrieved directly from the polycrystal simulations as functions of global Cu concentration. f_{GB} and a_0, in turn, were used to compute the crystal size a after doping and the longest possible shear band L.

The normalized flow stress estimated theoretically from Eq. (8) is presented as a function of the global composition in Fig. 9c. The theoretical estimate of normalized flow stresses in Ag-Cu alloys with homogeneous Cu segregation yields a saturation trend as a function of solute concentration, identical to that obtained numerically by atomistic simulation in Fig. 3c. This conclusion therefore validates that the flow stress saturation predicted in nanocrystalline Ag-Cu alloys is a salient feature of the competition between GB-induced strain-localization softening and GB-segregation strengthening.

4.3. Application to heterogeneous solute segregation

For heterogeneous Ni segregation in Ag, Fig. 9b, the Ni-rich clusters formed inside the sample obstruct the shear band, and thus shorten the possible length for shear localization. To keep our model simple, we assume that the Ni-rich clusters are all formed with a spherical shape of the same radius, r, at each triple junction of the GB network. The volume fraction of these clusters can be expressed as

$$f_{Cl} = \frac{6 \times \frac{1}{2}a_0^2\frac{\sqrt{3}}{2}}{6 \times \frac{1}{3}\pi r^2} = \frac{3\sqrt{3}a_0^2}{4\pi r^2}. \quad (9)$$

At low Ni composition, the clusters are too small to block the shear strain path, as schematically illustrated in Supplementary Materials Fig. S4. In this case, the length of the longest shear band is still formulated with Eq. (5). However, at high Ni composition, when the cluster is large enough to block the strain path, Fig. 9b, the longest shear strain length is reduced to

$$L = a_0 - 2r \quad (10)$$

For a given cluster volume fraction, Eq. (9) was used to calculate the cluster radius r and thus the length L from Eq. (10). Furthermore, based on Fig. 2b, the cluster volume fraction is a function of global composition. For homogeneous Cu segregation, the shear-band length increases as the GB atom volume fraction increases due to solute segregation. By contrast, the shear-band length in Ag-Ni alloys is shortened by the Ni-rich clusters and thus L decreases with increasing solute segregation. However, theoretical predictions from Eq. (8) should remain valid if the shear-band length L is estimated appropriately.

The normalized flow stress estimated theoretically is plotted in Fig. 9c as a function of the global Ni composition. The continuous increase of flow stress with no saturation with heterogeneous Ni segregation agrees well with the simulated MD trend obtained in Fig. 3c. Therefore, our model for shear-band strengthening by solute clustering qualitatively captures the solute-concentration dependence of flow stresses in nanocrystalline alloys with either homogeneous or heterogeneous segregation.

4.4. Implications of heterogeneous segregation

In their past work [14], Lu and coworkers studied the effects of Mo segregation on Hall-Petch strengthening and softening behaviors in nanocrystalline Ni-Mo alloys, finding that softening at fine grain sizes can eventually be reversed back to strengthening with increasing Mo concentration. The segregation pattern of Mo in the annealed nanocrystalline Ni-Mo alloys suggested strong heterogeneous Mo segregation to interfaces, albeit not explicitly stated as such by these authors. Despite the lack of direct experimental evidence, however, it is possible for us to assume that the heterogeneous segregation in the nanocrystalline Ni-Mo study could have played an active role on the continuous increase in plastic flow stresses with increasing Mo composition at extremely fine grain sizes, similarly to the present results in Ni-segregated nanocrystalline Ag.

The finding that heterogeneous segregation suppresses strain localization provides a new route to design tough materials through GB segregation engineering by not only increasing the strength as demonstrated above, but also by increasing the ductility. It is well known that strain localization leads to necking/shear banding, and eventually catastrophic failure in nanocrystalline materials, rendering nanocrystalline materials notoriously brittle despite the high strength [3]. The phenomenon presented here could be exploited in other alloys to improve the ductility of nanocrystalline materials, if the material system shows heterogeneous segregation behavior, while at the same time stabilizing the grain size.

5. Conclusion

The present computational and theoretical study has unveiled fundamental differences in GB-induced strengthening between homogeneous Cu segregation and heterogeneous Ni segregation in nanostructured Ag metals. It was shown that homogeneous and heterogeneous segregations both increase strength with different dependence on solute composition. Homogeneous Cu segregation increases the GB atom fraction forming a continuous strain path for shear localization, which leads to GB-induced softening and plastic flow stress saturation. In heterogeneous Ni segregation, however, the significant fraction of Ni-rich clusters with increasing Ni composition act as a reinforcing phase stopping strain localization at high strains. Generally, GB segregation engineering constitutes an important scientific breakthrough in the production of strong and stable nanocrystalline alloys [48–50]. The merit of heterogeneous segregation discovered here is to provide a unique solution for creating failure-resistant materials by segregation engineering. Heterogeneous segregation has been identified in several alloys such as Ag-Ni [22], Cu-Ta [19], Cu-Nb [42], Pt-Au [20], and Ni-Mo [14]. Therefore, these alloys offer promising opportunities to design stronger and tougher nanomaterials by this mechanism. In addition, heterogeneous segregation could potentially improve the tensile ductility of nanocrystalline materials that commonly exhibit rapid failure due to early necking or glass-like shear banding.

Declaration of Competing Interest

The authors declare that they have no known competing financial interests or personal relationships that could have appeared to influence the work reported in this paper.

Acknowledgments

This work received support from U.S. Department of Energy (DOE) Grant No. DE-SC0020054 and used the Supercomputer Cori of the National Energy Research Scientific Computing Center (NERSC), a U.S. DOE Office of Science User Facility operated under Contract No. DE-AC02–05CH11231.

Supplementary materials

Supplementary material associated with this article can be found, in the online version, at doi:10.1016/j.actamat.2020.08.074.

References

[1] N. Tsuji, Y. Ito, Y. Saito, Y. Minamino, Strength and ductility of ultrafine grained aluminum and iron produced by ARB and annealing, Scripta Mater 47 (12) (2002) 893–899.
[2] S. Cheng, E. Ma, Y.M. Wang, L.J. Kecskes, K.M. Youssef, C.C. Koch, U.P. Trociewitz, K. Han, Tensile properties of in situ consolidated nanocrystalline Cu, Acta Mater 53 (5) (2005) 1521–1533.
[3] M.A. Meyers, A. Mishra, D.J. Benson, Mechanical properties of nanocrystalline materials, Prog. Mater. Sci. 51 (4) (2006) 427–556.
[4] J. Schiotz, F.D. Di Tolla, K.W. Jacobsen, Softening of nanocrystalline metals at very small grain sizes, Nature 391 (1998) 561–563.
[5] H. Conrad, J. Narayan, On the grain size softening in nanocrystalline materials, Scripta Mater 42 (11) (2000) 1025–1030.
[6] S. Takeuchi, The mechanism of the inverse Hall-Petch relation of nanocrystals, Scripta Mater 44 (8) (2001) 1483–1487.
[7] J. Schiøtz, K.W. Jacobsen, A Maximum in the Strength of Nanocrystalline Copper, Science 301 (5638) (2003) 1357–1359.
[8] Z. Pan, Y. Li, Q. Wei, Tensile properties of nanocrystalline tantalum from molecular dynamics simulations Acta Mater. 56(14) (2008) 3470–3480
[9] J.R. Trelewicz, C.A. Schuh, The Hall–Petch breakdown in nanocrystalline metals: a crossover to glass-like deformation, Acta Mater 55 (17) (2007) 5948–5958.
[10] P.C. Millett, R.P. Selvam, A. Saxena, Improving grain boundary sliding resistance with segregated dopants, Mater. Sci. Eng. A 431 (1) (2006) 92–99.
[11] N. Du, Y. Qi, P.E. Krajewski, A.F. Bower, The Effect of Solute Atoms on Aluminum Grain Boundary Sliding at Elevated Temperature, Metall. Mater. Trans. A 42 (3) (2011) 651–659.
[12] R. Babicheva, S.V. Dmitriev, Y. Zhang, S.W. Kok, K. Zhou, Effect of Grain Boundary Segregation on Shear Deformation of Nanocrystalline Binary Aluminum Alloys at Room Temperature, Mater. Sci. Forum 838-839 (2016) 89–94.
[13] X. Ke, F. Sansoz, Segregation-affected yielding and stability in nanotwinned silver by microalloying, Phys. Rev. Mater. 1 (6) (2017) 063604.
[14] J. Hu, Y.N. Shi, X. Sauvage, G. Sha, K. Lu, Grain boundary stability governs hardening and softening in extremely fine nanograined metals, Science 355 (6331) (2017) 1292–1296.
[15] Z. Pan, T.J. Rupert, Effect of grain boundary character on segregation-induced structural transitions, Phys. Rev. B 93 (13) (2016) 134113.
[16] A.J. Detor, M.K. Miller, C.A. Schuh, Solute distribution in nanocrystalline Ni–W alloys examined through atom probe tomography, Phil. Mag. 86 (28) (2006) 4459–4475.
[17] A.J. Detor, C.A. Schuh, Grain boundary segregation, chemical ordering and stability of nanocrystalline alloys: atomistic computer simulations in the Ni–W system, Acta Mater 55 (12) (2007) 4221–4232.
[18] X. Ke, J. Ye, Z. Pan, J. Geng, M.F. Besser, D. Qu, A. Caro, J. Marian, R.T. Ott, Y.M. Wang, F. Sansoz, Ideal maximum strengths and defect-induced softening in nanocrystalline-nanotwinned metals, Nat. Mater. 18 (11) (2019) 1207–1214.
[19] T. Frolov, K.A. Darling, L.J. Kecskes, Y. Mishin, Stabilization and strengthening of nanocrystalline copper by alloying with tantalum, Acta Mater 60 (5) (2012) 2158–2168.
[20] C.J. O'Brien, C.M. Barr, P.M. Price, K. Hattar, S.M. Foiles, Grain boundary phase transformations in PtAu and relevance to thermal stabilization of bulk nanocrystalline metals, J. Mater. Sci. 53 (4) (2018) 2911–2927.
[21] P. Lu, F. Abdeljawad, M. Rodriguez, M. Chandross, D.P. Adams, B.L. Boyce, B.G. Clark, N. Argibay, On the thermal stability and grain boundary segregation in nanocrystalline PtAu alloys, Materialia 6 (2019) 100298.
[22] Z. Pan, V. Borovikov, M.I. Mendelev, F. Sansoz, Development of a semi-empirical potential for simulation of Ni solute segregation into grain boundaries in Ag, Model. Simul. Mater. Sci. Eng 26 (7) (2018) 075004.
[23] M.A. Gibson, C.A. Schuh, Segregation-induced changes in grain boundary cohesion and embrittlement in binary alloys, Acta Mater 95 (2015) 145–155.
[24] N.M. Heckman, S.M. Foiles, C.J. O'Brien, M. Chandross, C.M. Barr, N. Argibay, K. Hattar, P. Lu, D.P. Adams, B.L. Boyce, New nanoscale toughening mechanisms mitigate embrittlement in binary nanocrystalline alloys, Nanoscale 10 (45) (2018) 21231–21243.
[25] C.C. Koch, D.G. Morris, K. Lu, A. Inoue, Ductility of Nanostructured Materials, MRS Bulletin 24 (02) (1999) 54–58.
[26] Q. Wei, D. Jia, K.T. Ramesh, E. Ma, Evolution and microstructure of shear bands in nanostructured Fe, Appl. Phys. Lett. 81 (7) (2002) 1240–1242.
[27] Y. Wang, M. Chen, F. Zhou, E. Ma, High tensile ductility in a nanostructured metal, Nature 419 (6907) (2002) 912–915.
[28] A. Hasnaoui, H. Van Swygenhoven, P.M. Derlet, Dimples on Nanocrystalline Fracture Surfaces As Evidence for Shear Plane Formation, Science 300 (5625) (2003) 1550–1552.
[29] K.S. Kumar, H. Van Swygenhoven, S. Suresh, Mechanical behavior of nanocrystalline metals and alloys, Acta Mater 51 (19) (2003) 5743–5774.
[30] F. Sansoz, V. Dupont, Atomic mechanism of shear localization during indentation of a nanostructured metal, Mater. Sci. Eng. C 27 (5) (2007) 1509–1513.
[31] A. Khalajhedayati, T.J. Rupert, Emergence of localized plasticity and failure through shear banding during microcompression of a nanocrystalline alloy, Acta Mater 65 (2014) 326–337.
[32] T.J. Rupert, Strain localization in a nanocrystalline metal: atomic mechanisms and the effect of testing conditions, J. Appl. Phys. 114 (3) (2013) 033527.
[33] P. Hua, K. Chu, Q. Sun, Grain refinement and amorphization in nanocrystalline NiTi micropillars under uniaxial compression, Scripta Mater 154 (2018) 123–126.
[34] Y. Wang, C. Huang, Y. Li, F. Guo, Q. He, M. Wang, X. Wu, R. Scattergood, Y. Zhu, Dense dispersed shear bands in gradient-structured Ni, Int. J. Plasticity (2019) 124.
[35] K.S. Kormout, B. Yang, R. Pippan, Deformation Behavior and Microstructural Evolution of Cu–Ag Alloys Processed by High-Pressure Torsion, Adv. Eng. Mater. 17 (12) (2015) 1828–1834.
[36] G.H. Balbus, F. Wang, D.S. Gianola, Suppression of shear localization in nanocrystalline Al–Ni–Ce via segregation engineering, Acta Mater 188 (2020) 63–78.
[37] S. Plimpton, Fast Parallel Algorithms for Short-Range Molecular Dynamics, J. Comp. Phys. 117 (1) (1995) 1–19.
[38] H.H. Wu, D.R. Trinkle, Cu/Ag EAM potential optimized for heteroepitaxial diffusion from ab initio data, Comput. Mater. Sci. 47 (2) (2009) 577–583.
[39] J.D. Honeycutt, H.C. Andersen, Molecular dynamics study of melting and freezing of small Lennard-Jones clusters, J. Phys. Chem. 91 (19) (1987) 4950–4963.
[40] A. Stukowski, Visualization and analysis of atomistic simulation data with OVITO–the Open Visualization Tool, Model. Simul. Mater. Sci. Eng 18 (1) (2010) 015012.
[41] B. Sadigh, P. Erhart, A. Stukowski, A. Caro, E. Martinez, L. Zepeda-Ruiz, Scalable parallel Monte Carlo algorithm for atomistic simulations of precipitation in alloys, Phys. Rev. B 85 (18) (2012) 184203.
[42] Z. Pan, T.J. Rupert, Formation of ordered and disordered interfacial films in immiscible metal alloys, Scripta Mater 130 (2017) 91–95.
[43] A. Li, I. Szlufarska, Morphology and mechanical properties of nanocrystalline Cu/Ag alloy, J. Mater. Sci. 52 (8) (2017) 4555–4567.
[44] A. Inoue, W. Zhang, T. Tsurui, A.R. Yavari, A.L. Greer, Unusual room-temperature compressive plasticity in nanocrystal-toughened bulk copper-zirconium glass, Phil. Mag. Lett. 85 (5) (2005) 221–237.
[45] T. Brink, K. Albe, From metallic glasses to nanocrystals: molecular dynamics simulations on the crossover from glass-like to grain-boundary-mediated deformation behaviour, Acta Mater 156 (2018) 205–214.
[46] S.D. Feng, L. Li, K.C. Chan, L. Qi, L. Zhao, L.M. Wang, R.P. Liu, Control of shear band dynamics in Cu50Zr50 metallic glass by introducing amorphous-crystalline interfaces, J. Alloys Comp 770 (2019) 896–905.
[47] J. Gruber, H. Lim, F. Abdeljawad, S. Foiles, G.J. Tucker, Development of physically based atomistic microstructures: the effect on the mechanical response of polycrystals, Computational Materials Science 128 (2017) 29–36.
[48] T. Chookajorn, H.A. Murdoch, C.A. Schuh, Design of Stable Nanocrystalline Alloys, Science 337 (6097) (2012) 951–954.
[49] D. Raabe, S. Sandlöbes, J. Millán, D. Ponge, H. Assadi, M. Herbig, P.P. Choi, Segregation engineering enables nanoscale martensite to austenite phase transformation at grain boundaries: a pathway to ductile martensite, Acta Mater 61 (16) (2013) 6132–6152.
[50] D. Raabe, M. Herbig, S. Sandlöbes, Y. Li, D. Tytko, M. Kuzmina, D. Ponge, P.P. Choi, Grain boundary segregation engineering in metallic alloys: a pathway to the design of interfaces, Curr. Opin. Solid St. M. 18 (4) (2014) 253–261.